# An essential role for the Hv1 voltage-gated proton channel in *Pseudomonas aeruginosa* corneal infection

Priscila Rodriguez[1] , Serena Abbondante[2], Michaela Marshall[2], Jessica Abdelmeseh[1], Francesco Tombola[1*], and Eric Pearlman[1, 2*]

[1]Department of Physiology and Biophysics, [2]Department of Ophthalmology, University of California, Irvine, Irvine, CA

*co-corresponding authors eric.pearlman@uci.edu, ftombola@uci.edu

**ABSTRACT**

Assembly of NADPH oxidase 2 (NOX2) proteins in neutrophils plays an essential role in controlling microbial infections by producing high levels of reactive oxygen species (ROS). In contrast, the role of the Hv1 voltage-gated proton channel that is required for sustained NOX2 activity is less well characterized. We examined the role of Hv1 in a murine model of blinding *Pseudomonas aeruginosa* corneal infection and found that in contrast to C57BL/6 mice, *Hvcn1*$^{-/-}$ mice exhibit an impaired ability to kill bacteria and regulate disease severity. *In vitro*, we used a novel Hv1 Inhibitor Flexible (HIF) to block ROS production by human and murine neutrophils and found that HIF inhibits ROS production in a dose-dependent manner following stimulation with PMA or infection with *P. aeruginosa*. Collectively, these findings demonstrate an important role for Hv1 on controlling bacterial growth in a clinically relevant bacterial infection model.

## Introduction

Microbial infections of the cornea are among the leading causes of preventable blindness world-wide and *Pseudomonas aeruginosa* is a major cause of corneal infections in the USA and worldwide. Contact lens wear is the main risk factor in industrialized countries, whereas ocular trauma is the major predisposing cause in developing countries [1]. These infections result in corneal opacity, inflammation, and intense pain that can lead to permanent blindness if left untreated. While antibiotics are the first line of defense, there are increasing reports of antibiotic resistance in clinical isolates of *P. aeruginosa*, including a 2023 outbreak of drug resistant *P. aeruginosa* keratitis due to a contaminated artificial tears product that was imported to the USA. As of March 2023, there were 68 patients from 16 states who were infected with this virulent strain, resulting in 3 deaths and 8 enucleations [2, 3]. Although these eyedrops have been withdrawn from use, this outbreak illustrates the importance of developing antimicrobial and anti-inflammatory therapies as corneal opacification is also due to cellular infiltration and inflammation. Our collaborative studies at the Aravind Eye Hospital in Tamil Nadu, India identified neutrophils as the major cell types (>90%) infiltrating corneal ulcers caused by *P. aeruginosa, Streptococcus pneumoniae* or pathogenic fungi [4, 5]. Consistent with these reports, we reported that neutrophils are the predominant cell type in infected corneas in a murine models of *P. aeruginosa* keratitis, and that neutrophil depletion resulted in impaired bacterial killing and corneal ulceration [6, 7].

Neutrophils utilize both oxidative and non-oxidative effectors to kill bacteria, including iron and zinc binding proteins that compete with bacterial siderophores and transporters, potent phagocytic activity and release of extracellular traps containing DNA and microbicidal histones [8, 9]. However, reactive oxygen species (ROS) play an outsized role in bacterial killing, especially following phagocytosis and formation of phagolysosomes.

Neutrophil ROS production in phagolysosomes is primarily generated by the NADPH oxidase protein complex 2 (NOX2) that includes the $gp91^{phox}$ and $p22^{phox}$ proteins on plasma and

phagosome membranes, which together with Rac small G protein comprise the flavocytochrome b558 (cytb558) subunit. The regulatory $p40^{phox}$, $p47^{phox}$ and $p67^{phox}$ proteins in the cytoplasm translocate to the membrane following phosphorylation of $p47^{phox}$ and associates with cytb558 to form NOX2 (reviewed in [10] ). Once assembled, NOX2 generates ROS superoxide ($O_2^-$) by accepting electrons from cytoplasmic NADPH and donating them to molecular oxygen, leading to membrane depolarization and accumulation of protons in the cytoplasm, which in turn leads to acidification of the cytosol. The importance of NOX2 for bacterial killing has been well described in patients with mutations in these subunits, most commonly $gp91^{phox}$, who are highly susceptible to infection [11]. We also reported that mice with deletions in $gp91^{phox}$ are unable to control blinding bacterial and fungal infections of the cornea [12, 13].

Although a role for NADPH oxidase in regulating microbial infections has been well documented, there are relatively few reports on the role of the Hv1 voltage-gated proton channel and its role in sustaining NADPH activity in neutrophils (reviewed in [14]). The Hv1 proton channel is a membrane protein that maintains cellular pH homeostasis by releasing protons across the plasma and the phagosome membranes. The protein has four transmembrane segments folded in a proton-conducting voltage-sensing domain (VSD) that resembles the corresponding domain of voltage-gated sodium, potassium, and calcium channels [15, 16]. While NOX2 activity is inhibited by membrane depolarization and cytosolic acidification, Hv1 is activated under these same conditions and releases $H^+$ ions into the phagolysosome, thereby sustaining NOX2 mediated ROS production. El Chemaly and colleagues reported that in the absence of Hv1, neutrophil and macrophage phagosomes exhibit impaired ROS production [17].

In the current study, we used *Hvcn1*$^{-/-}$ mice to examine the role of Hv1 in a clinically relevant murine model of blinding *Pseudomonas aeruginosa* corneal infection (keratitis). We found that *Hvcn1*$^{-/-}$ mice exhibit an impaired ability to clear *P. aeruginosa* from infected corneas compared to C57BL/6 mice, thereby demonstrating the importance of Hv1 and sustained ROS production during bacterial infection. As Hv1 activity is associated with increased severity of

neurological disease including spinal cord and traumatic brain injury, and ischemic stroke (reviewed in [15, 16]), there is a strong interest in developing Hv1 inhibitors as potential anti-inflammatory therapies. One promising small molecule compound is Hv1 Inhibitor Flexible (HIF), which was recently identified as an effective Hv1 inhibitor, binds the channel VSD in the closed and open conformation, thereby blocking its proton conduction pathway [18]. Our current findings show that HIF blocks ROS production by human and murine neutrophils infected with *P. aeruginosa* or following stimulation with PMA or fungal cell wall extracts.

## 2. MATERIALS AND METHODS

### 2.1 Mice

Male and female C57BL/6J mice aged 6-8 weeks were purchased from The Jackson Laboratory (Bar Harbor, ME). Two *Hvcn1*$^{-/-}$ breeding pairs were graciously provided from Dr. Long-Jun Wu and colleagues, Mayo Clinic, Rochester, MN [19]. Mice were housed in the University of California, Irvine vivarium. Age-matched, male and female mice were used for all experiments, and the experimental protocol was approved by the UC Irvine IACUC.

### 2.2 Bacterial strains and culture conditions

PAO1, PAO1-GFP and Δ*pscD* were obtained from Dr. Arne Rietsch (Case Western Reserve University). Bacteria were grown to mid-log phase (~1× $10^8$ bacteria/ml) in high-salt Luria-Bertani (LB) broth, at 37°C with 5% $CO_2$. Bacteria were washed and suspended in 1x PBS to a final concentration of 5×$10^4$ bacteria/2 µl for *in vivo* infections and 3x$10^8$ (MOI 30) for *in vitro* assays.

### 2.3 Murine model of *Pseudomonas* keratitis

Corneal epithelial abrasions (3 x 5mm) were made using a sterile 30-gauge needle followed by topical infection with 5×$10^4$ PAO1-GFP in 2 µl in PBS as described previously [20] . CFU was quantified after 2h to verify the inoculum for each experiment. After 24h, mice were

euthanized and corneal opacity and GFP fluorescence were imaged and quantified by image analysis (ImageJ, NIH).

**2.4 Imaging of infected mouse corneas**

Mice were euthanized by $CO_2$ asphyxiation followed by cervical dislocation and were positioned in a 3-point stereotactic mouse restrainer for eye imaging. Corneal opacity (brightfield [BF]) and bacterial burden (GFP) were visualized in the intact cornea using a high-resolution stereo fluorescence MZFLIII microscope (Leica Microsystems). ImageJ was then used to calculate corneal opacity and GFP intensity. All images were obtained using the same LAS V4.5 Software under the same magnification (×20), exposure (BF, 0.4 seconds; eGFP, 2 seconds), gain (BF, 1; RFP/eGFP, 4/16), and gamma (BF/RFP/eGFP, 1.85) parameters.

**2.5 CFU Quantification**

At 2 (inoculum) or 24h post infection, whole eyes were collected and homogenized in 1 ml PBS using a 5mm steel ball bearing and Qiagen TissueLyser II at 30 Hz for 3 minutes. Serial log dilutions (10 µl) of the homogenate were plated on LB agar plates and incubated overnight at 37°C with 5% $CO_2$. Colonies were counted manually, and viable bacteria were calculated as CFU/ml: number of colonies × dilution factor × 100.

**2.6 Flow cytometry**

Dissected corneas were incubated in 500 µl of 3 mg/ml collagenase (C0130; SigmaAldrich) in RPMI (Gibco), with 1% HEPES (Gibco), 1% penicillin-streptomycin (Gibco), 0.5% BSA (Fisher Bioreagents), and 2 µl of 1M Calcium Chloride for 1 h at 37°C. Cells were incubated for 10 min with anti-mouse CD16/32 Ab (BioLegend) to block Fc receptors. Cells were then incubated 20 min at 4°C with anti-mouse CD45-PE-Cy5, Ly6G-BV510, Ly6C-PE-Cy7, CD11b-PETxRed, CCR2-BV421, and F4/80-FITC (BioLegend) and fixable viability dye e780 (BD Biosciences). Cells were rinsed with FACS buffer and fixed with Cytofix/Cytoperm (BD Biosciences) for 15 min at 4°C. Fixed cells were washed with PBS and resuspended in FACS buffer. Data were analyzed using NovoExpress software.

### 2.7 Cytokine quantification

At the experimental endpoint, infected corneas were resected and placed in a 2 ml tube containing 500 µl of sterile 1x PBS (Corning) and a sterile 5mm steel ball bearing. Corneas were lysed using a Qiagen TissueLyser II at 30 Hz for 3 minutes. Samples were then centrifuged at 16,0000 x g for 10 minutes at 4°C and cell free supernatant was carefully removed. R&D Systems mouse DuoSet ELISA kits were used and manufacturer protocol was followed. ELISA plates were read on an Agilent (BioTek) Cytation5.

### 2.8 Histology and immunohistochemistry (IHC)

Whole eyes were fixed in Davidson Fixative (Polysciences) for 24h before transitioning to 70% ethanol. Paraffin embedding and sectioning was done by the UCI Optical Microanatomy Core where tissue blocks were cut into 8 µM sections. Sections were deparaffinized and hydrated to water before staining with hematoxylin and eosin (Fisher Scientific) and were imaged on an Olympus BX60 with a Diagnostic Instruments camera attachment. For IHC, slides were deparaffinized and hydrated to water and antigen retrieval was done via proteinase K (Agilent, Dako) incubation at 37°C for 20 minutes. Sections were washed in PBS, permeabilized in 1% Tween-20 in PBS (PBST, Fisher Bioreagents), and were then incubated 1 hour with Fc block (BioLegend) and normal goat serum (Jackson ImmunoResearch) diluted in 1% BSA (Fisher Bioreagents). Primary antibodies: Ly-6G/Ly-6C Monoclonal Antibody NIMP-R14 (Invitrogen) and Rabbit anti-H3Cit (Abcam) were diluted 1:50 and 1:100, respectively, in blocking buffer and incubated overnight at 4°C. Slides were washed 3x for 10 minutes with PBS. Secondary antibodies goat anti-Rat 647 (Invitrogen) and goat anti-Rabbit 488 (Invitrogen) were diluted 1:1000 and 1:500, respectively, in blocking buffer and added to sections for 1 hour at RT protected from light. Slides were then washed 4x for 10 minutes in PBS and counterstained with DAPI. Finally, slides were mounted using Vectashield® Antifade Mounting Medium (Vector Laboratories) and were examined and imaged on a Leica Stellaris 8 confocal microscope. Image processing was done using LAS X (Leica) and ImageJ (NIH) software.

### 2.9 Human and Murine Neutrophil Isolation

Total human blood was acquired through the UC Irvine Institute for Clinical and Translational Science Blood Donor program under an approved IRB protocol. Blood was first incubated with 3% Dextran (Sigma Aldrich) for 18 minutes for erythrocyte sedimentation. The top layer of cells, which includes plasma, neutrophils, PBMCs and some remaining erythrocytes, was transferred to a 50 ml conical tube and 10 ml of Ficoll-paque plus (Cytiva, Fisher Scientific) was carefully underlaid. Samples were then centrifuged at 500 x g for 30 minutes at 20°C. Following centrifugation, three distinct layers form: top plasma layer, middle PBMC layer, and bottom neutrophil/erythrocyte pellet. Erythrocytes from the pellet were lysed with chilled RBC lysis buffer (eBioscience), and remaining neutrophils were counted manually and resuspended at $1x10^6$ in RPMI 1640 without phenol red (Gibco).

Mouse whole bone marrow was removed from the femur and tibia bones via centrifugation and was resuspended in 500 µl of chilled EasySep™ buffer (Stemcell). Bone marrow neutrophils were then isolated using the Stemcell EasySep™ Mouse Neutrophil Isolation Kit following the manufacturers protocol. Mouse neutrophils were counted manually and resuspended at $1x10^6$ in RPMI 1640 without phenol red (Gibco).

### 2.10 Reactive Oxygen Species Assay

Neutrophils were isolated as detailed above and were incubated at 37°C with 5% $CO_2$ in RPMI 1640 without phenol red (Gibco) with 500 µM Luminol (Sigma Aldrich) for 30 minutes before stimulation. Neutrophils were added to black sided, optically clear bottom 96-well plates (Corning) at $2x10^5$/well and DPI (Sigma Aldrich) was added to respective wells at a final concentration of 10 µM for 15 minutes prior to stimulation. *P. aeruginosa* (MOI), curdlan (100 ug/ml, Sigma Aldrich), PMA (100 ug/ml, Sigma Aldrich), and zymosan (100 ug/ml, Invivogen) were added and the plate was immediately read on a Cytation5 plate reader (Agilent, BioTek) for 90 minutes at 37°C, taking luminescent (Lum) readings every 2 minutes. Time course curves

were generated by the Cytation5 Gen5 software and area under the curve was calculated from the time course using GraphPad Prism Software.

### 2.11 Hv1 Inhibitor Flexible (HIF)

HIF, or 3-(2-amino-5-methyl-1*H*-imidazol-4-yl)-1-(3,5-difluorophenyl)propan-1-one, a small molecule Hv1 inhibitor consisting of an aminoimidazole ring, and an fluorinated aromatic group connected by an extended flexible linker (refs. 12-13 ) was custom synthesized by Enamine and SynInnova at a minimum purity of 95%, determined by liquid chromatography-mass spectrometry. Stock solutions were **prepared** in dry DMSO at a concentration of 50 or 100 mM and stored a 4°C under desiccant. Final solutions in RPMI or PBS were freshly prepared by dilution from stocks.

### 2.12 Statistics

For *in vivo* experiments, statistical significance was determined using paired t-tests (GraphPad Prism). *In vitro* assays required a minimum of 3 biological repeats using the mean of 4 technical replicates. Error bars indicate mean ± SEM and p values less than 0.05 are considered significant. The number of biological replicates for each experiment can be found in the figure legends.

## 3. RESULTS

### Hv1 regulates disease severity and bacterial killing in a murine model of blinding *Pseudomonas aeruginosa* cornea infection

We reported that GP91$^{PHOX}$ /CybB$^{-/-}$ mice are unable to kill *P. aeruginosa* in infected corneas, resulting in more severe disease [13], thereby demonstrating that NADPH oxidase and ROS are required to regulate bacterial growth. As Hv1 sustains release of ROS generated by NOX2, we assessed the role of the Hv1 voltage-gated proton channel in *P. aeruginosa* keratitis. The corneal epithelium of C57BL/6 and *Hvcn1*$^{-/-}$ mice was abraded and infected topically with $5\times10^4$ *P. aeruginosa* strain PAO1 that expresses Green Fluorescent Protein as we recently

described [20, 21]. After 24h, corneal opacity and GFP+ bacteria were quantified by image analysis, and CFU was used as a measure of bacterial viability.

Although corneal opacification was observed in both strains of mice, infected *Hvcn1*$^{-/-}$ corneas had significantly elevated corneal opacity and total bacterial mass (GFP) (**Figure 1A-C)**. Viable bacteria (CFU) were also significantly higher in infected *Hvcn1-/-* compared with C57BL/6 corneas (**Figure 1D)**. Collectively, these results show that disease is exacerbated in *Hvcn1-/-* mice compared to control mice and therefore indicate that the Hv1 proton channel is required to clear PAO1 infection, likely by sustaining NOX2 activity.

**Impaired bacterial killing in the absence of Hv1 is not due to increased neutrophil recruitment to infected corneas**

The healthy corneal stroma has resident dendritic cells and macrophages, but no neutrophils. However, following *P. aeruginosa* infection, there is a pronounced cell recruitment to infected corneas from peripheral limbal vessels and from the highly vascularized iris. This results in >90% CD45+ myeloid cells, primarily neutrophils and inflammatory monocytes [20]. As Hv1 can promote neutrophil migration by regulating calcium signaling [17], we examined the effect of Hv1 deficiency on neutrophil recruitment to infected corneas by immunohistochemistry and flow cytometry.

Corneas of C57BL/6 and *Hvcn1*$^{-/-}$ were infected with *P. aeruginosa* as described above, and after 24h, eyes were fixed in Davidson Fixative and 8 µm sections were stained with hematoxylin and eosin to detect cellular infiltration in relation to the whole cornea. In addition, sections were incubated with antibodies to identify neutrophils (Ly6G) and citrullinated histone 3 (H3Cit) as an indicator of neutrophil extracellular traps (NETs).

There was a pronounced cellular infiltrate in the corneal stroma, epithelium and lining the anterior chamber of C57BL/6 and *Hvcn1*$^{-/-}$ corneas (**Figure 2A)**. Neutrophils were the predominat cell type in infected corneas at this early time point, many of which formed NETs in the corneal

stroma; however, there was no apparent difference in neutrophil numbers between C57BL/6 and *Hvcn1*$^{-/-}$ mice (**Figure 2B)**.

To quantify the number of neutrophils and monocytes in infected corneas, we dissected individual corneas and digested them with collagenase. Single cell suspensions were then incubated with antibodies to monocytes (CD45+/CD11b+/Ly6G-) and neutrophils CD45+/CD11b+/Ly6G+), which were then quantified by flow cytometry. The gating strategy is shown in **Figure S1**.

We found that neutrophils comprised ~85-90% of the total cellular infiltrate in infected C57BL/6 corneas, with 10-15% monocytes. However, there was no significant difference in the number or percentage of infiltrating neutrophils or monocytes in *Hvcn1*$^{-/-}$ and C57BL/6 mice (**Figure 2C,D).**

In conclusion, the elevated number of viable bacteria in infected *Hvcn1*$^{-/-}$ corneas is not due to impaired recruitment of neutrophils, but is instead consistent with a compromised ability of *Hvcn1*$^{-/-}$ neutrophils to kill *P. aeruginosa in vivo*.

**Elevated cytokine production in infected *Hvcn1*$^{-/-}$ corneas**

*P. aeruginosa* infection of corneas induces pro-inflammatory and chemotactic cytokine production by resident macrophages, epithelial cells and keratocytes to initially recruit circulating myeloid cells, which then produce these cytokines in response to replicating bacteria [22]. To assess the effect of Hv1 deficiency on cytokine production in *P. aeruginosa* infected corneas, *Hvcn1*$^{-/-}$ and C57BL/6 corneas were infected with PAO1 and after 24h corneas were processed using a bead homogenizer. Following centrifugation, cytokines in the cell free supernatants were quantified by ELISA. As shown in **Figure 3,** production of IL-1α, IL-1β and CXCL1 was significantly higher in infected *Hvcn1*$^{-/-}$ corneas compared to C57BL/6 mice. CXCL2 was also elevated in *Hvcn1*$^{-/-}$ corneas, although the difference was not statistically significant.

Given that the same number of neutrophils infiltrate infected *Hvcn1*$^{-/-}$ as C57BL/6 corneas, we interpret the increase in proinflammatory cytokine production in infected *Hvcn1*$^{-/-}$ corneas as a consequence of the increased number of bacteria that continue to induce cytokine production.

**Hv1 Inhibitor Flexible (HIF) blocks ROS production by human and murine neutrophils**

We reported that *P. aeruginosa* ExoS inhibits NOX2 activity and ROS production by human neutrophils through ADP ribosylation of RAS; consequently, ROS is generated following infection with the T3SS injectosome mutant Δ*pscD,* which does not form a needle structure and therefore cannot inject ExoS or other exoenzymes into the host cell cytosol [13].

To examine the role of Hv1 on ROS production in infected corneas, we used a novel Hv1 voltage-gated proton inhibitor called HIF (Hv1 Inhibitor Flexible) that directly interacts with the voltage sensing domains of the channel in the open and closed conformation [18, 23]. To determine if HIF blocks ROS production by infected neutrophils, bone marrow neutrophils from C57BL/6 mice and human peripheral blood neutrophils from healthy donors were isolated by negative bead selection and Ficoll gradient, respectively, and were incubated with increasing concentrations of HIF. Neutrophils were either incubated with phorbol myristate acetate (PMA), or infected with the Type III secretion mutant Δ*pscD* for 90 minutes in the presence of Luminol. As we reported, ExoS ADP ribosyl transferase produced by the parent strain PAO1 inhibits NADPH oxidase assembly and ROS production following infection whereas ROS is produced in response to the mutant Δ*pscD* that does not produce ExoS [8]. As a control for total ROS production, neutrophils were also incubated with the NOX2 inhibitor Diphenyleneiodonium (DPI).

We found that DPI completely blocked ROS production as expected, but also that HIF inhibited ROS production in Δ*pscD* infected neutrophils in a dose – dependent manner (**Figure 4A,B).** Similarly, HIF inhibited ROS production by peripheral blood human neutrophils stimulated with PMA or infected with Δ*pscD* (**Figure 4C,D)**. HIF also inhibited ROS production induced by

murine and peripheral blood human neutrophils stimulated with insoluble β-glucan curdlan or zymosan, and we reproduced our earlier findings that PAO1 does not induce ROS production (**Figure S4, 5)**. Collectively, these results indicate that HIF acts downstream of PKC activation, consistent with the role of Hv1 in relieving cellular proton accumulation generated by sustained NOX2 activity.

## 4. DISCUSSION

Hv1 is the only known voltage-gated proton channel in mammals, and in contrast to other voltage gated channels, Hv1 is unique in not having a pore domain and also in its response to mechanical stress [24-26]. Hv1 expression in B lymphocytes contributes to ROS dependent B cell receptor activation and antibody production [27]; however, there are relatively few reports on the role of Hv1 in neutrophils. Ramsay et al generated *Hvcn1*$^{-/-}$ mice and showed that following intraperitoneal infection with $1x10^8$ or $1x10^9$ *Staphylococcus aureus*, there were more bacteria recovered from *Hvcn1*$^{-/-}$ mice than WT mice after 6h, although there was no difference at 24h post infection [25]. In contrast to our findings, Okochi and co-workers reported that *Hvcn1*$^{-/-}$ mice infected intranasally with *Candida albicans* had elevated pulmonary inflammation, but there was no effect of Hv1 deficiency on fungal killing [28].

In the current study, we used a clinically relevant murine model of *P. aeruginosa* corneal infection, where neutrophils comprise >80% of the total cellular infiltrate, similar to patients with corneal ulcers [4, 5]. We demonstrated that the Hv1 voltage-gated proton channel is required to clear *Pseudomonas aeruginosa* corneal infection as *Hvcn1*$^{-/-}$ mice have more severe corneal opacity resulting from increased bacterial growth. The difference between Okochi's findings and ours likely involves the site of infection (lungs vs. corneas) and requirements to kill pathogenic bacteria compared with fungi.

Recruitment of neutrophils and monocytes to infected corneas requires adhesion to and transmigration across capillary endothelial cells, and migration between the collagen fibrils of the

stroma. El Chemaly *et al*. reported that Hv1 was necessary for efficient migration of neutrophils using an *in vitro* spreading and motility assay in response to agonists of formyl peptide receptors [17]. However, we found no difference in the total number of neutrophils or monocytes per cornea in *Hvcn1*$^{-/-}$ compared with C57BL/6 mice, indicating that the higher bacterial count in infected *Hvcn1*$^{-/-}$ mice is intrinsic to the ability of neutrophils to kill *P. aeruginosa*.

Our current findings extend those from a previous report from our lab demonstrating that ROS production by human neutrophils was required to kill bacteria *in vitro,* and that GP91$^{PHOX}$ deficient mice also have an impaired ability to clear *P. aeruginosa* from infected corneas, which resulted in more severe ocular disease [13]. That study also showed that the type III secretion (T3SS) exoenzyme S (ExoS) blocked ROS production by ADP ribosylation of the Ras small GTPase required for recruitment of cytosolic NOX proteins and thereby inhibiting NOX2 assembly at the phagolysosome membrane and allowing growth of T3SS mutants in corneas of GP91$^{PHOX}$ deficient mice that do not grow or cause disease in WT mice.

The HIF compound was expected to inhibit the fraction of Hv1 channels on the cell surface in addition to the channels localized to the phagosomes. The compound needs to cross the plasma membrane to reach the intracellular region of the VSD where it binds [18, 23]. Compared to other small molecule Hv1 inhibitors like ClGBI [29], HIF has the advantage that binding does not require the channel to be active. Compared to Hv1 peptide inhibitors, such as C6 that can suppress pulmonary inflammation [30-33], HIF has increased cell permeability. Accordingly, we found that HIF effectively inhibits ROS production in neutrophils infected with *P. aeruginosa* Δ*pscD* mutant that induces ROS production. We found that HIF also blocked ROS production induced by fungal cell wall components in curdlan and zymosan, and by PMA.

In conclusion, these findings identify a critical role for Hv1 in sustaining ROS production by neutrophils to kill pathogenic *P. aeruginosa* in a clinically relevant model of blinding corneal infection. This role for Hv1 occurs even as *P. aeruginosa* ExoS inhibits NADPH oxidase assembly, indicating that Hv1 can compensate for the effect of ExoS. As bacterial keratitis is a

major cause of corneal disease where neutrophils contribute to degradation of the stromal matrix, targeting Hv1 with inhibitors such as HIF may reduce the inflammation and fibrosis associated with infection. The current treatment comprises topical antibiotics to kill the bacteria, followed by corticosteroids to limit inflammation [34]. However, when corticosteroids are combined with an ineffective antimicrobial treatment, bacteria replication is uncontrolled due to the suppressed immune response, resulting in more severe disease that may require corneal transplantation. Additionally, there are undesirable side effects when treating with corticosteroids such as increased intraocular pressure and increased risk for glaucoma; therefore, Hv1 proton channel inhibitors represent a novel target for anti-inflammatory therapies that would follow antibiotic treatment.

## Author contributions

PR, SA, JA and MEM performed all experiments and generated graphs and images. FT produced HIF for all experiments. PR, SA, FT and EP designed the experiments and wrote the manuscript.


## Acknowledgements

We would like to thank Dr. Chang Zhao (UCI) for initial tests of Hv1 inhibitors on ROS production in human neutrophils, and Dr. Liang Hong (University of Illinois, Chicago) for help with raising initial *HVCN1*$^{-/-}$ breeding pairs.


## Author declarations

**Ethics approval:** All animal studies were approved by the UC Irvine IACUC. Volunteer blood donors signed informed consent forms as part of the healthy blood donor program at UC Irvine managed by the Institute for Clinical and Translation Research.

**Competing interests**

The authors declare no conflicts of interest.


**Funding:** These studies were supported by NIH grants R01 EY14362 (EP) and R01 GM098973 (FT) The authors also acknowledge departmental support from an unrestricted grant to the Department of Ophthalmology from the Research to Prevent Blindness Foundation, New York, NY.

## References


1. Ung, L., Bispo, P. J. M., Shanbhag, S. S., Gilmore, M. S., Chodosh, J. (2019) The persistent dilemma of microbial keratitis: Global burden, diagnosis, and antimicrobial resistance. Surv Ophthalmol 64, 255-271.
2. Morelli, M. K., Kloosterboer, A., Fulton, S. A., Furin, J., Newman, N., Omar, A. F., Rojas, L. J., Marshall, S. H., Yasmin, M., Bonomo, R. A. (2023) Investigating and Treating a Corneal Ulcer Due to Extensively Drug-Resistant Pseudomonas aeruginosa. Antimicrob Agents Chemother, e0027723.
3. Morelli, M. K., Kloosterboer, A., Omar, A. F. (2023) Pseudomonas aeruginosa Corneal Ulcer Associated With Artificial Tears Eye Drops. JAMA Ophthalmol 141, 496.
4. Karthikeyan, R. S., Priya, J. L., Leal, S. M., Jr., Toska, J., Rietsch, A., Prajna, V., Pearlman, E., Lalitha, P. (2013) Host response and bacterial virulence factor expression in Pseudomonas aeruginosa and Streptococcus pneumoniae corneal ulcers. PLoS One 8, e64867.
5. Karthikeyan, R. S., Leal, S. M., Jr., Prajna, N. V., Dharmalingam, K., Geiser, D. M., Pearlman, E., Lalitha, P. (2011) Expression of innate and adaptive immune mediators in human corneal tissue infected with Aspergillus or fusarium. J Infect Dis 204, 942-50.
6. Karmakar, M., Katsnelson, M., Malak, H. A., Greene, N. G., Howell, S. J., Hise, A. G., Camilli, A., Kadioglu, A., Dubyak, G. R., Pearlman, E. (2015) Neutrophil IL-1beta processing induced by pneumolysin is mediated by the NLRP3/ASC inflammasome and caspase-1 activation and is dependent on K+ efflux. J Immunol 194, 1763-75.
7. Karmakar, M., Sun, Y., Hise, A. G., Rietsch, A., Pearlman, E. (2012) Cutting edge: IL-1beta processing during Pseudomonas aeruginosa infection is mediated by neutrophil serine proteases and is independent of NLRC4 and caspase-1. J Immunol 189, 4231-5.
8. Murdoch, C. C. and Skaar, E. P. (2022) Nutritional immunity: the battle for nutrient metals at the host-pathogen interface. Nat Rev Microbiol 20, 657-670.

9. Brinkmann, V., Reichard, U., Goosmann, C., Fauler, B., Uhlemann, Y., Weiss, D. S., Weinrauch, Y., Zychlinsky, A. (2004) Neutrophil extracellular traps kill bacteria. Science 303, 1532-5.

10. Bode, K., Hauri-Hohl, M., Jaquet, V., Weyd, H. (2023) Unlocking the power of NOX2: A comprehensive review on its role in immune regulation. Redox Biol 64, 102795.

11. Yu, H. H., Yang, Y. H., Chiang, B. L. (2021) Chronic Granulomatous Disease: a Comprehensive Review. Clin Rev Allergy Immunol 61, 101-113.

12. Leal, S. M., Jr., Vareechon, C., Cowden, S., Cobb, B. A., Latge, J. P., Momany, M., Pearlman, E. (2012) Fungal antioxidant pathways promote survival against neutrophils during infection. J Clin Invest 122, 2482-98.

13. Vareechon, C., Zmina, S. E., Karmakar, M., Pearlman, E., Rietsch, A. (2017) Pseudomonas aeruginosa Effector ExoS Inhibits ROS Production in Human Neutrophils. Cell Host Microbe 21, 611-618 e5.

14. Okochi, Y. and Okamura, Y. (2021) Regulation of Neutrophil Functions by Hv1/VSOP Voltage-Gated Proton Channels. Int J Mol Sci 22.

15. Shen, Y., Luo, Y., Liao, P., Zuo, Y., Jiang, R. (2023) Role of the Voltage-Gated Proton Channel Hv1 in Nervous Systems. Neurosci Bull 39, 1157-1172.

16. He, J., Ritzel, R. M., Wu, J. (2021) Functions and Mechanisms of the Voltage-Gated Proton Channel Hv1 in Brain and Spinal Cord Injury. Front Cell Neurosci 15, 662971.

17. El Chemaly, A., Okochi, Y., Sasaki, M., Arnaudeau, S., Okamura, Y., Demaurex, N. (2010) VSOP/Hv1 proton channels sustain calcium entry, neutrophil migration, and superoxide production by limiting cell depolarization and acidification. J Exp Med 207, 129-39.

18. Zhao, C., Hong, L., Riahi, S., Lim, V. T., Tobias, D. J., Tombola, F. (2021) A novel Hv1 inhibitor reveals a new mechanism of inhibition of a voltage-sensing domain. J Gen Physiol 153.

19. Wu, L. J., Wu, G., Akhavan Sharif, M. R., Baker, A., Jia, Y., Fahey, F. H., Luo, H. R., Feener, E. P., Clapham, D. E. (2012) The voltage-gated proton channel Hv1 enhances brain damage from ischemic stroke. Nat Neurosci 15, 565-73.

20. Ratitong, B., Marshall, M. E., Dragan, M. A., Anunciado, C. M., Abbondante, S., Pearlman, E. (2022) Differential Roles for IL-1alpha and IL-1beta in Pseudomonas aeruginosa Corneal Infection. J Immunol 209, 548-558.

21. Minns, M. S., Liboro, K., Lima, T. S., Abbondante, S., Miller, B. A., Marshall, M. E., Tran Chau, J., Roistacher, A., Rietsch, A., Dubyak, G. R., Pearlman, E. (2023) NLRP3 selectively drives IL-1beta secretion by Pseudomonas aeruginosa infected neutrophils and regulates corneal disease severity. Nat Commun 14, 5832.

22. Sun, Y., Karmakar, M., Roy, S., Ramadan, R. T., Williams, S. R., Howell, S., Shive, C. L., Han, Y., Stopford, C. M., Rietsch, A., Pearlman, E. (2010) TLR4 and TLR5 on corneal macrophages regulate Pseudomonas aeruginosa keratitis by signaling through MyD88-dependent and -independent pathways. J Immunol 185, 4272-83.

23. Zhao, C., Hong, L., Galpin, J. D., Riahi, S., Lim, V. T., Webster, P. D., Tobias, D. J., Ahern, C. A., Tombola, F. (2021) HIFs: New arginine mimic inhibitors of the Hv1 channel with improved VSD-ligand interactions. J Gen Physiol 153.

24. Sasaki, M., Tojo, A., Okochi, Y., Miyawaki, N., Kamimura, D., Yamaguchi, A., Murakami, M., Okamura, Y. (2013) Autoimmune disorder phenotypes in Hvcn1-deficient mice. Biochem J 450, 295-301.

25. Ramsey, I. S., Moran, M. M., Chong, J. A., Clapham, D. E. (2006) A voltage-gated proton-selective channel lacking the pore domain. Nature 440, 1213-6.

26. Pathak, M. M., Tran, T., Hong, L., Joos, B., Morris, C. E., Tombola, F. (2016) The Hv1 proton channel responds to mechanical stimuli. J Gen Physiol 148, 405-418.

27. Capasso, M., Bhamrah, M. K., Henley, T., Boyd, R. S., Langlais, C., Cain, K., Dinsdale, D., Pulford, K., Khan, M., Musset, B., Cherny, V. V., Morgan, D., Gascoyne, R. D.,

Vigorito, E., DeCoursey, T. E., MacLennan, I. C., Dyer, M. J. (2010) HVCN1 modulates BCR signal strength via regulation of BCR-dependent generation of reactive oxygen species. Nat Immunol 11, 265-72.

28. Okochi, Y., Aratani, Y., Adissu, H. A., Miyawaki, N., Sasaki, M., Suzuki, K., Okamura, Y. (2016) The voltage-gated proton channel Hv1/VSOP inhibits neutrophil granule release. J Leukoc Biol 99, 7-19.

29. Hong, Y. R., Kim, H. T., Ro, S., Cho, J. M., Lee, S. H., Kim, I. S., Jung, Y. H. (2014) Discovery of novel 2-[2-(3-hydroxy-pyridin-2-yl)-thiazol-4-yl]-acetamide derivatives as HIF prolyl 4-hydroxylase inhibitors; SAR, synthesis and modeling evaluation. Bioorg Med Chem Lett 24, 3142-5.

30. Hong, L., Pathak, M. M., Kim, I. H., Ta, D., Tombola, F. (2013) Voltage-sensing domain of voltage-gated proton channel Hv1 shares mechanism of block with pore domains. Neuron 77, 274-87.

31. Zhao, R., Shen, R., Dai, H., Perozo, E., Goldstein, S. A. N. (2022) Molecular determinants of inhibition of the human proton channel hHv1 by the designer peptide C6 and a bivalent derivative. Proc Natl Acad Sci U S A 119, e2120750119.

32. Zhao, R., Lopez, B., Schwingshackl, A., Goldstein, S. A. N. (2023) Protection from acute lung injury by a peptide designed to inhibit the voltage-gated proton channel. iScience 26, 105901.

33. Zhao, R., Dai, H., Arias, R. J., De Blas, G. A., Orta, G., Pavarotti, M. A., Shen, R., Perozo, E., Mayorga, L. S., Darszon, A., Goldstein, S. A. N. (2021) Direct activation of the proton channel by albumin leads to human sperm capacitation and sustained release of inflammatory mediators by neutrophils. Nat Commun 12, 3855.

34. Cabrera-Aguas, M., Khoo, P., Watson, S. L. (2022) Infectious keratitis: A review. Clin Exp Ophthalmol 50, 543-562.

## FIGURE LEGENDS

**Figure 1. Role of Hv1 in *Pseudomonas aeruginosa* keratitis.** Corneas of C57BL/6 and *Hvcn1-/-* mice were infected with $5 \times 10^4$ GFP expressing PAO1 bacteria and examined after 24h. A. Representative images of corneal opacification (brightfield) and GFP-PAO1 in infected C57BL/6 and *Hvcn1-/-* mice. Inset: healthy, transparent mouse cornea. B. Quantification of corneal opacity by image analysis using Image J. C. Total GFP+ bacteria in infected corneas quantified by image analysis. D. Viable bacteria quantified by CFU, n=12, three experiments combined. Statistical significance was calculated using paired t-test, n=12, combined data from three independent experiments.

**Figure 2. Neutrophil and monocyte recruitment into PAO1 infected corneas.** Corneas of C57BL/6 and *Hvcn1-/-* mice were infected with $5 \times 10^4$ PAO1/2 µl PBS. 24h post infection, corneas were dissected and digested in collagenase, and the number of neutrophils and monocytes was assessed by flow cytometry. Eyes were embedded in paraffin and 8µm sections were stained with H&E. A) Representative flow cytometry plots of live, single, CD45+ cells. Neutrophils were identified as Ly6G+CD11b+ and monocytes were identified as CD11b+Ly6G- cells. B) Quantification of neutrophils and monocytes as a percentage of total CD45+ cells. n=6 infected mice, two experiments combined. C) Representative images of H&E stained corneal sections of PA01 infected corneas. D) IHC showing neutrophils and neutrophil extracellular traps (NETs). Original magnification is x200.

**Figure 3. Cytokine production in *Hvcn1-/-* infected corneas.** Corneas of C57BL/6 and *Hvcn1-/-* mice were infected with $5 \times 10^4$ *P. aeruginosa* in 2 µl PBS. After 24h, corneas were homogenized, centrifuged, and pro-inflammatory cytokines and chemokines were quantified by

ELISA. Statistical significance was calculated using paired t-test, and $p<0.05$ was considered significant.

**Figure 4. HIF inhibits extracellular ROS production in a dose-dependent manner in human and murine neutrophils.** A-D: Murine bone marrow neutrophils were incubated with 500 μM luminol and Hv1 Inhibitor Flexible (HIF) or DPI and either stimulated with 100 μM phorbol myristate acetate (PMA)(A, B), or infected with the *P. aeruginosa* type III secretion mutant Δ*pscD*. Left panels: representative time course of ROS production measured as relative fluorescent units (RFU) per second; right panels: area under the curve calculated from 3-6 biological replicates. F-H: Human peripheral blood neutrophils incubated in the same conditions as murine neutrophils. No inhibitor compared with all HIF concentrations or with DPI is $p<0.05$.

**Figure 1**

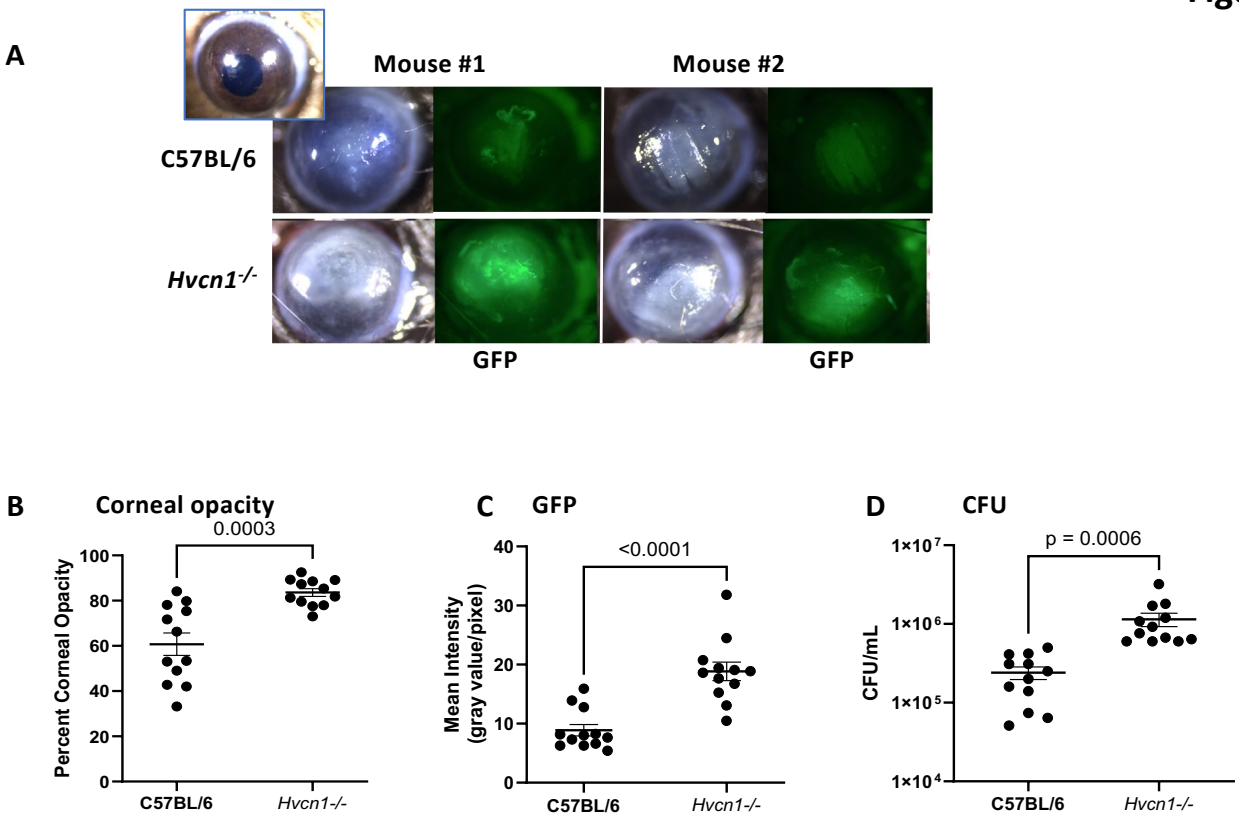
A
Mouse #1
Mouse #2
C57BL/6
Hvcn1-/-
GFP
GFP
B
Corneal opacity
0.0003
Percent Corneal Opacity
100
80
60
40
20
0
C57BL/6
Hvcn1-/-
C
GFP
<0.0001
Mean Intensity
(gray value/pixel)
40
30
20
10
0
C57BL/6
Hvcn1-/-
D
CFU
p = 0.0006
CFU/mL
1×10⁷
1×10⁶
1×10⁵
1×10⁴
C57BL/6
Hvcn1-/-

# Figure 2

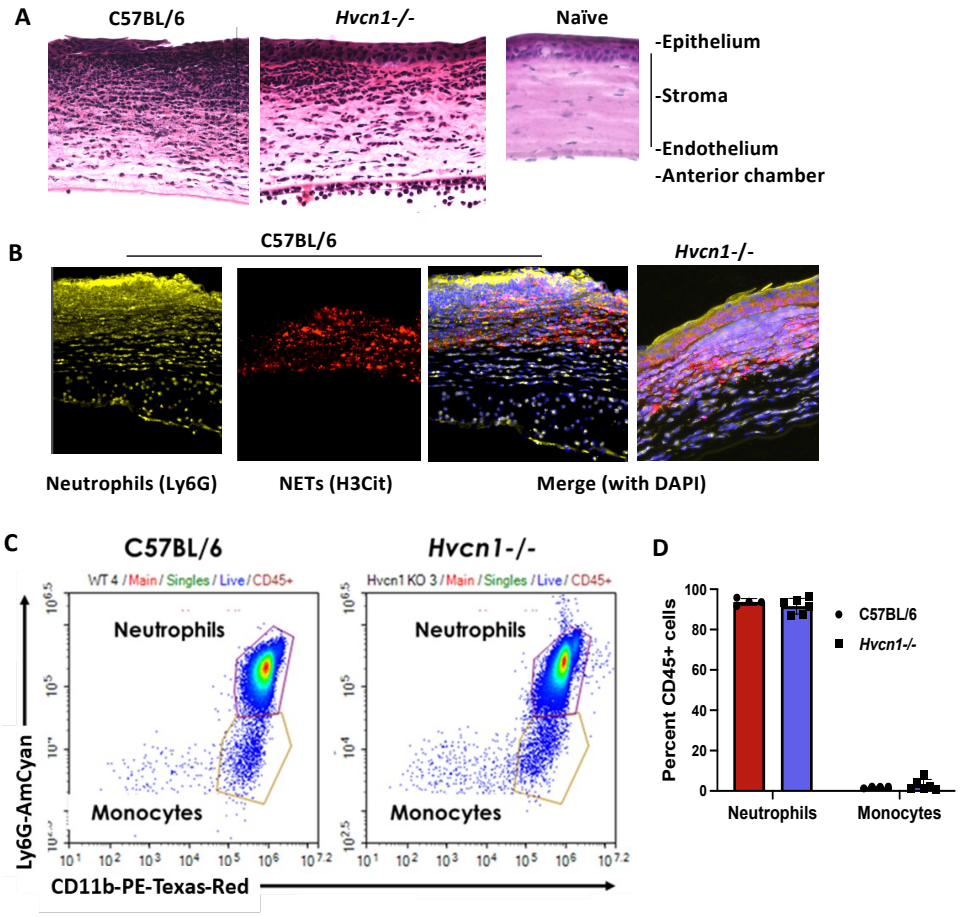
A
C57BL/6
Hvcn1-/-
Naïve
-Epithelium
-Stroma
-Endothelium
-Anterior chamber
B
C57BL/6
Hvcn1-/-
Neutrophils (Ly6G)
NETs (H3Cit)
Merge (with DAPI)
C
C57BL/6
Hvcn1-/-
WT 4 / Main / Singles / Live / CD45+
Hvcn1 KO 3 / Main / Singles / Live / CD45+
Neutrophils
Monocytes
Ly6G-AmCyan
CD11b-PE-Texas-Red
D
Percent CD45+ cells
C57BL/6
Hvcn1-/-
Neutrophils
Monocytes

**Figure 3**

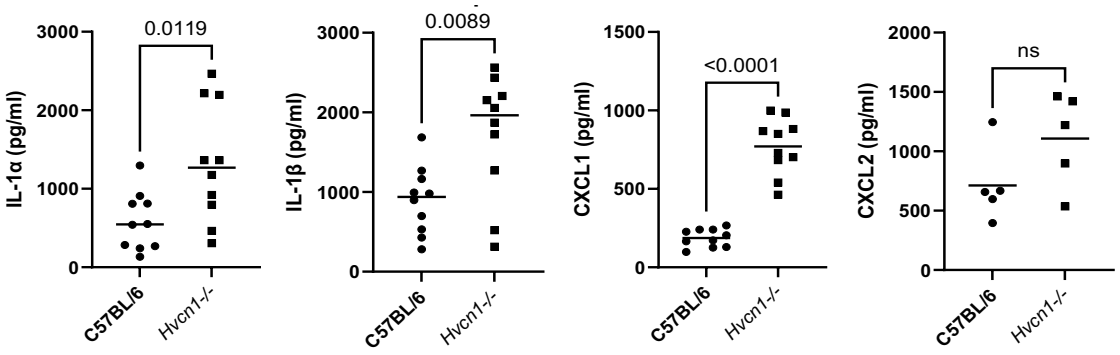
IL-1α (pg/ml)
3000
2000
1000
0
0.0119
C57BL/6
Hvcn1-/-
IL-1β (pg/ml)
3000
2000
1000
0
0.0089
C57BL/6
Hvcn1-/-
CXCL1 (pg/ml)
1500
1000
500
0
<0.0001
C57BL/6
Hvcn1-/-
CXCL2 (pg/ml)
2000
1500
1000
500
0
ns
C57BL/6
Hvcn1-/-

Figure 4

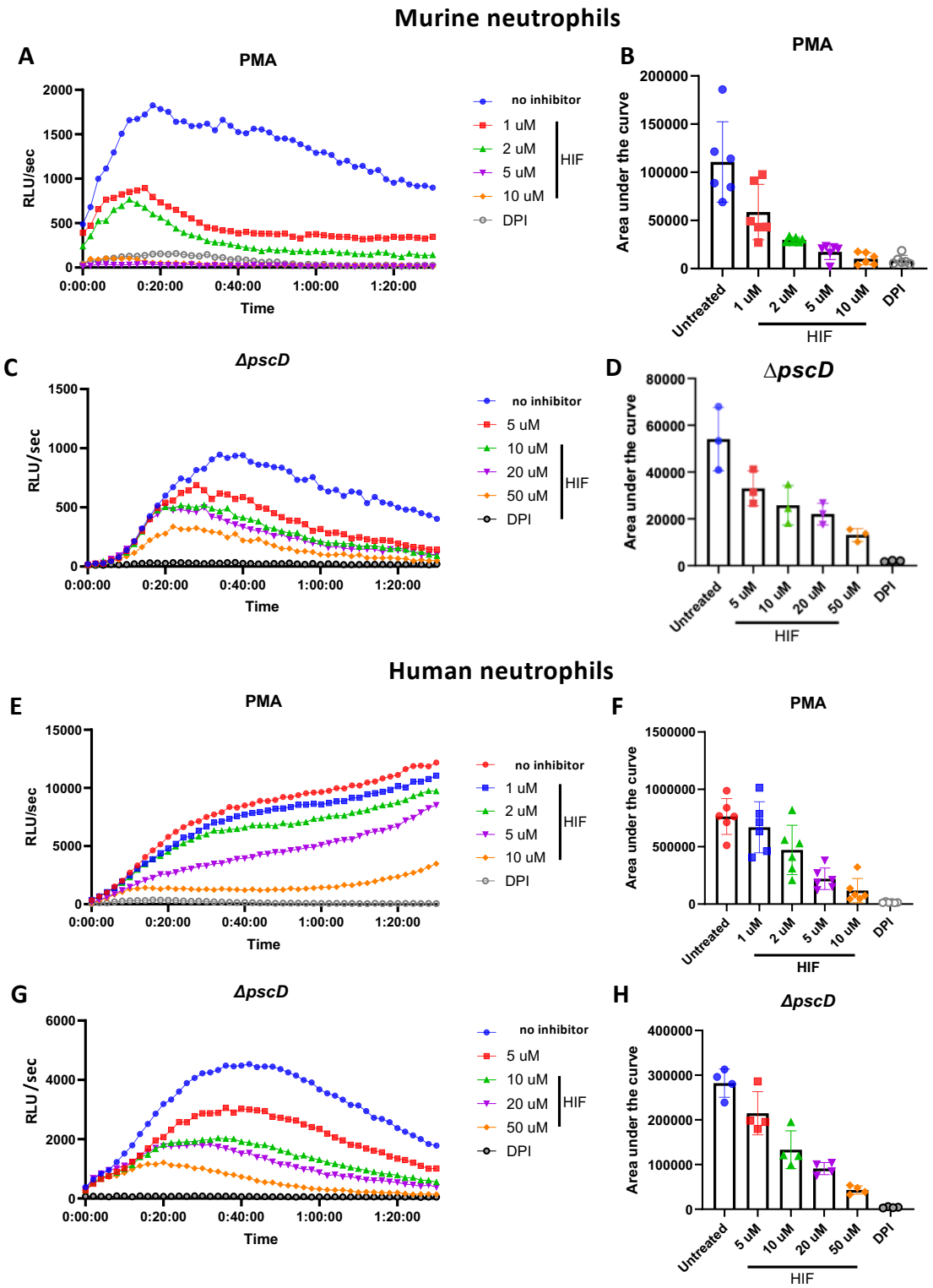
Murine neutrophils
A
PMA
RLU/sec
Time
no inhibitor
1 uM
2 uM
5 uM
10 uM
DPI
HIF
B
PMA
Area under the curve
Untreated
1 uM
2 uM
5 uM
10 uM
DPI
HIF
C
ΔpscD
RLU/sec
Time
no inhibitor
5 uM
10 uM
20 uM
50 uM
DPI
HIF
D
ΔpscD
Area under the curve
Untreated
5 uM
10 uM
20 uM
50 uM
DPI
HIF
Human neutrophils
E
PMA
RLU/sec
Time
no inhibitor
1 uM
2 uM
5 uM
10 uM
DPI
HIF
F
PMA
Area under the curve
Untreated
1 uM
2 uM
5 uM
10 uM
DPI
HIF
G
ΔpscD
RLU /sec
Time
no inhibitor
5 uM
10 uM
20 uM
50 uM
DPI
HIF
H
ΔpscD
Area under the curve
Untreated
5 uM
10 uM
20 uM
50 uM
DPI
HIF